Journal of the Korean Nuclear Society
Volume 35, Number 4, pp. 274~285, August 2003

Film Boiling Heat Transfer from Relatively Large Diameter Downward-facing Hemispheres

Chan Soo Kim, Kune Y. Suh, Goon Cherl Park, and Un Chul Lee
Seoul National University
San 56-1 Shillim-dong, Kwanak-gu, Seoul, 151-742, Korea
kysuh@snu.ac.kr

Ho Jun Yoon
Purdue University
West Lafayette, IN 47907, USA

(Received October 24, 2002)

Abstract

Film boiling heat transfer coefficients for a downward-facing hemispherical surface are measured from the quenching tests in DELTA (Downward-boiling Experimental Loop for Transient Analysis). Two test sections are made of copper to maintain Bi below 0.1. The outer diameters of the hemispheres are 120 mm and 294 mm, respectively. The thickness of both the test sections is 30 mm. The effect of diameter on film boiling heat transfer is quantified utilizing results obtained from the two test sections. The measured heat transfer coefficients for the test section with diameter 120 mm lie within the bounding values from the laminar film boiling analysis, while those for diameter 294 mm are found to be greater than the numerical results on account of the Helmholtz instability. There is little difference observed between the film boiling heat transfer coefficients measured from the two test sections. In addition, the higher thermal conductivity of copper results in the higher minimum heat flux in the tests. For the test section of diameter 120 mm, the Leidenfrost point is lower than that for the test section of diameter 294 mm. Destabilization of film boiling propagates radially inward for the 294 mm test section versus radially outward for the 120 mm Test Section.

Key Words : film boiling, downward-facing hemisphere, interfacial wavy motion

1. Introduction

In the process of design for the APR1400 (Advanced Power Reactor 1400 MWe), the in-vessel retention through external vessel cooling (IVR-EVC) was chosen as a severe accident management strategy. Cavity flooding was selected as the external vessel cooling method because of the relatively simpler installation than that of flooding within the thermal insulator. In fact, the IVR-EVC concept had not been considered during the initial design phase of the APR1400. Thus several issues surfaced while applying the IVR concept at a later stage of

design. One of these issues centered about delayed flooding of the reactor vessel because of the large volume between the cavity floor and the lower head. The cavity flooding and flooding within the thermal insulator may take as much as forty minutes. It is thus not certain whether the flooding time be shorter than that of relocation of the molten core material down to the lower plenum of the reactor vessel. In addition, the initial temperature of the vessel will be in the neighborhood of the saturated temperature corresponding to the accident pressure condition. Hence, the initial heat removal mechanism for external vessel cooling will most likely be film rather than nucleate boiling. It turned out, however, that film boiling heat transfer coefficients presently available in the literature tend to underpredict the actual value for the reactor vessel lower head.

Bromley [1], Koh [2], Sparrow and Cess [3], and Nishikawa and Ito [4] investigated film boiling on vertical plates. They applied the various boundary conditions to prediction of film boiling heat transfer coefficients. Generally, the boundary conditions at the interface between the vapor film and bulk liquid were divided into zero interfacial velocity and the same interfacial shear stress. Frederking and Clark [5], Sakurai et al. [6], and Tou and Tso [7] studied models for the laminar film boiling heat transfer coefficients on spheres based on the previous analytic solutions for those on the vertical plates.

The film boiling heat transfer coefficients were measured higher for relatively long vertical plate than those predicted for the laminar film boiling [8]. Dhir and Purohit [9] measured the film boiling heat transfer coefficients 50~60 % higher than those predicted by the laminar plane interface theory for spheres. Kolev [10] developed the correlation with the Helmholtz instability at vertical plates and spheres. Kim [11] performed experiments with nickel-plated copper spheres of various diameters to study film boiling heat transfer and its stability in flowing water. Experimental data are nonexistent for the downward-facing hemisphere on a large scale, however.

In this study, film boiling heat transfer coefficients are obtained from the quenching test apparatus DELTA (Downward-boiling Experimental Loop for Transient Analysis) utilizing the measured temperature values.

2. Laminar Film Boiling Analysis

The assumptions adopted in this analysis include the incompressible flow model, the Boussinesq approximation, negligible inertia and convection terms, the laminar film layer, fluid motion in the boundary layer only, temperature-independent vapor thermophysical properties, negligible viscous heating, stable and thin film layer, smooth wall surface, and negligible effects of interfacial wave. The computational procedure proposed by Tou and Tso [7] is applied in this study to solve for the laminar film boiling heat transfer on the hemispherical test sections adopted in DELTA.

The governing equations for the vapor film in the spherical coordinate system take on the following forms

$$\frac{\partial}{\partial\theta}(u\sin\theta)=0 \tag{1}$$

$$\frac{\mu_v}{r^2}\frac{\partial}{\partial r}\left(r^2\frac{\partial u}{\partial r}\right)=g(\rho_l-\rho_v)\sin\theta \tag{2}$$

$$\frac{1}{r^2}\frac{\partial}{\partial r}\left(r^2\frac{\partial T}{\partial r}\right)=0 \tag{3}$$

Two boundary conditions are applied for the analytical solution. Case 1 assumes that the velocity is zero at the liquid-vapor interface. Case

2 surmises that the interfacial shear stress has the same value in the vapor film and in the bulk liquid and that the value is small enough to be neglected. The boundary conditions other than the interfacial velocity and shear stress include Frederking and Clark' s conditions[5]. The boundary conditions are thus taken as

Solid Wall (r=R)

$$u = 0 \tag{4}$$

$$T = T_w \tag{5}$$

$$-k_v \frac{\partial T}{\partial r} 2\pi R^2 \sin\theta = h_{lv} dw_i \tag{6}$$

Interface (r=R+δ)

$$T = T_{sat} \tag{7}$$

$$dw_v = dw_l = dw_i = d\left(\int_R^{R+\delta} \rho_v u 2\pi R \sin\theta dr \right) \tag{8}$$

$$u = 0 \rightarrow case\ 1 \tag{9}$$

$$\tau_v = \tau_l = -\mu_v \frac{\partial u}{\partial r} = 0 \rightarrow case\ 2 \tag{10}$$

Equations (4) and (5) show that the vapor velocity is zero and its temperature is equal to the wall temperature on the wall surface. Equation (6) signifies that all the heat transferred from the surface to vapor film is consumed for vaporization of the liquid to develop the vapor film boundary layer. Equation (7) implies that the vapor temperature at the interface is equal to the saturated temperature. Equation (8) suggests that the vapor mass flow rate is equal to the liquid mass flow rate at the interface and in the increased boundary layer. Equations (9) and (10) present the velocity boundary conditions for cases 1 and 2, respectively. The velocity and temperature profiles are derived from Equations (2), (3), (4), (5), (7), (9) and (10). The local thickness of the film layer is determined from Equations (6) and (8). It is assumed that the vapor thickness at the bottom (θ = 0°) is zero. The film boiling heat transfer coefficient for case 1 is lower than that in case 2. Table 1 presents the velocity profiles, interfacial mass flow rate, and angular vapor film thickness for cases 1 and 2.

The heat transfer from a differential area at the wall-vapor interface in case 1 is calculated from

$$dq = k_v \left(-\frac{\partial T}{\partial r} \right)_{r=R} 2\pi R^2 \sin\theta d\theta = \frac{k_v \Delta T \pi R (1+\delta/R) \left[\int_0^\theta \sin^{5/3}\theta d\theta \right]^{-0.25}}{[8Ja/Ra]^{0.25}} \tag{11}$$

The total heat transfer from the hemisphere is found by integrating Equation (11) from the bottom (θ= 0°) to the top (θ= 90°) as

$$q = \frac{k_v \Delta T \pi R}{\left[Ra/8Ja \right]^{-0.25}} \left\{ \int_0^{\pi/2} \sin^{5/3}\theta \left[\int_0^\theta \sin^{5/3}\theta d\theta \right]^{-0.25} d\theta + \int_0^{\pi/2} \frac{\delta}{R} \sin^{5/3}\theta \left[\int_0^\theta \sin^{5/3}\theta d\theta \right]^{-0.25} d\theta \right\} \tag{12}$$

The average Nu is evaluated from Equation (12) as

$$Nu = \left[\frac{Ra}{8Ja} \right]^{0.25} \left\{ \int_0^{\pi/2} \sin^{5/3}\theta \left[\int_0^\theta \sin^{5/3}\theta d\theta \right]^{-0.25} d\theta + \int_0^{\pi/2} \frac{\delta}{R} \sin^{5/3}\theta \left[\int_0^\theta \sin^{5/3}\theta d\theta \right]^{-0.25} d\theta \right\} \tag{13}$$

The average Nu is finally determined by plugging the vapor film thickness in Table 1 into Equation (13) as

$$Nu = 1 + 0.696 \left(Ra/Ja \right)^{0.25} \tag{14}$$

Table 1. Velocity Profiles, Interfacial Mass Flow Nate, and Angular Vapor Film Thickness

Velocity Profile	*zero velocity*	$u=\frac{-g(\rho_l-\rho_v)\sin\theta}{6\mu_v}\left[r^2+\frac{2R^3+3R^2\delta+R\delta^2}{r}-3R^2-3R\delta-\delta^2\right]$
	same interfacial τ	$u=\frac{-g(\rho_l-\rho_v)\sin\theta}{3\mu_v}\left[\frac{r^2}{2}+\frac{(R+\delta)^3}{r}-\frac{R^2}{2}-\frac{(R+\delta)^3}{R}\right]$
Interfacial Mass Flow Rate	*zero velocity*	$dw_i=\frac{2\pi RRak_v}{96c_p}d\left[\sin^2\theta\left(\frac{\delta}{R}\right)^3\right]$
	same interfacial τ	$dw_i=\frac{2\pi RRak_v}{24c_p}d\left[\sin^2\theta\left(\frac{\delta}{R}\right)^3\right]$
Angular film Thickness Distribution	*zero velocity*	$\frac{\delta}{R}=2\left[8\frac{Ja}{Ra}\right]^{0.25}\frac{\left[\int_0^\theta\sin^{5/3}\theta d\theta\right]^{0.25}}{\sin^{2/3}\theta}$
	same interfacial τ	$\frac{\delta}{R}=\left[32\frac{Ja}{Ra}\right]^{0.25}\frac{\left[\int_0^\theta\sin^{5/3}\theta d\theta\right]^{0.25}}{\sin^{2/3}\theta}$

for case 1.

The coefficient 0.696 in Equation (14) is replaced by 0.985 for case 2. The vapor properties utilized in Ra and Ja are evaluated at the film temperature

$$T_f=\frac{T_w+T_{sat}}{2} \tag{15}$$

An effective latent heat term [5] is generally used for correction of sensible heat as

$$h_{lv}^*=h_{lv}+0.5c_{p,v}\Delta T_{sat} \tag{16}$$

3. Experimental Loop and Data Reduction

Figure 1 presents the cross-sectional view of the test sections with diameters of 120 mm and 294 mm, respectively. The diameters of the stainless steel and Fire Stop disk on the test section respectively are 118 mm and 292 mm which are smaller than diameters of the two copper hemispheres. This explains why difference in thermal expansion of the three different materials does not interfere with release of bubbles on the top of the hemispheres. Figure 2 shows the thermocouples installed at 0°, 20°, 40°, 60° and 80° near the outer surface and the inner surface of both test sections. The thermocouples were calibrated in ISOTECH TRU (Temperature Reference Unit) Model 740. The holes were drilled through the center of the stainless steel disk, stainless steel pipe, and the Fire Stop to route the wall thermocouples to the HP-VXI E1413C data acquisition system. The test section is made of copper to maintain Bi below 0.1 in the film boiling regime. In case of Bi less than 0.1 the conduction heat transfer in the solid may be neglected [12]. Thus, the experimental data could be compared with numerical analysis for the isothermal hemispherical surface. The thickness of the copper vessel was 3 cm for data from the quenching experiment to equal those from the

steady state experiment [13]. If the time to traverse the top 10 % of the boiling curve was greater than 1 sec, the boiling process was in a quasi-steady state [14]. The test section' s inner cavity was filled with bulk fiber and covered on top with the Fire Stop disk for thermal insulation. A stainless steel disk was fastened to the test section wall using the stainless steel bolts.

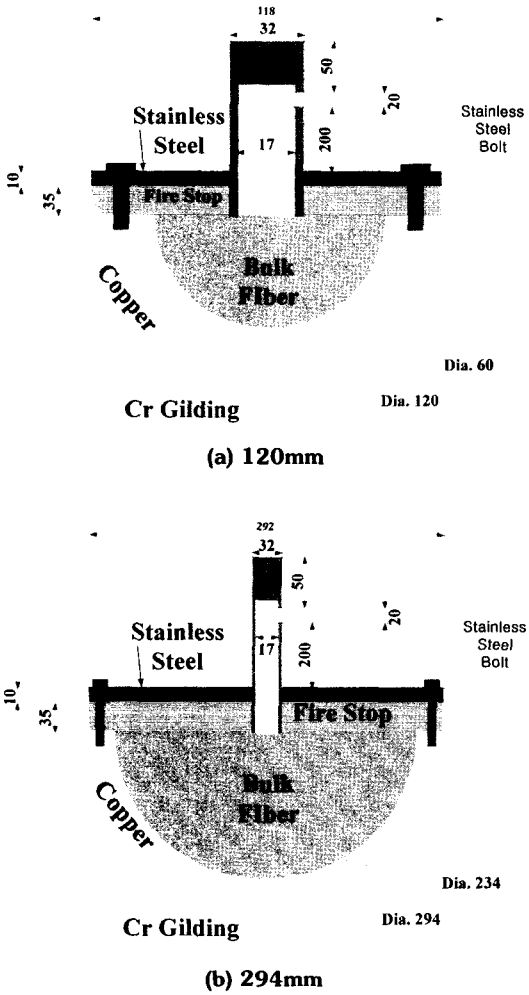

Fig. 1. Cross-sectional View of Test Sections

The hexahedral quenching tank is of 1.00 × 1.00° × 1.10m. A tank must have 3.5 times the dimension of the test section to maintain pool boiling without the effect of the quenching tank size [15]. It has a large glass window on one side for visual inspection and recording of the pool boiling on the hemispherical surface during quenching using a video camera. During the experiment, the water in the tank was maintained at the saturated condition utilizing four 10 kW and two 7 kW heaters.

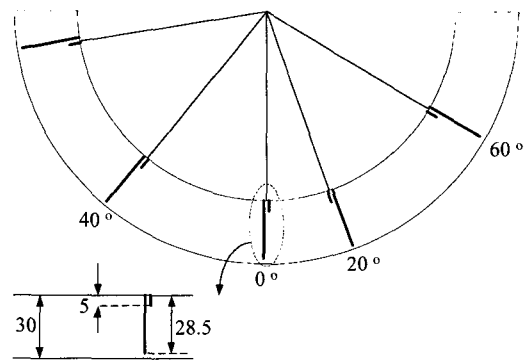

Fig. 2. Azimuthal Locations of Thermocouples (length unit: mm)

Prior to each quenching experiment, the demineralized water in the tank was degassed by boiling for thirty minutes. The test section was heated up to 280oC. The heated test section was transferred from the furnace to the quenching tank by an automatic lift for a few seconds. The heated test section was then submerged in the quenching tank with its top surface kept 10 cm below the water level. Figure 3 shows the experimental apparatus DELTA.

This experiment was designed for measurement of temperature profile pursuant to the film boiling heat transfer coefficient. Measured temperature history was smoothed by means of a 10 point FFT-filter in Microcal Origin 6.0. The film boiling heat transfer coefficient was calculated from the smoothed temperature history as follows

$$h_{film} = \frac{\rho c_P G \Delta T}{\Delta t \Delta T_{sat}} - 0.75 h_{rad} \qquad (17)$$

Pursuant to Equation (17), the heat transfer coefficient is determined by the wall temperature rate of change during the time step, wall superheat, and a geometrical parameter as well as material properties. The local temperature difference is small such that the conduction heat transfer has to be neglected in the test sections so as to minimize uncertainties in the estimated film boiling heat transfer coefficients.

$$\frac{U_{h_{film}}}{h_{film}} = \frac{\sqrt{2}U_T}{\Delta T} \tag{18}$$

4. Results and Discussion

In the experiments, all the local temperature difference was found to stay within ± 0.5℃ in the film boiling regime, because the thermal conductivity of the test sections was high enough. Hence the conduction heat transfer could be neglected in obtaining the film boiling heat transfer coefficient. The average standard deviation of the film boiling heat transfer coefficient was ±8 %.

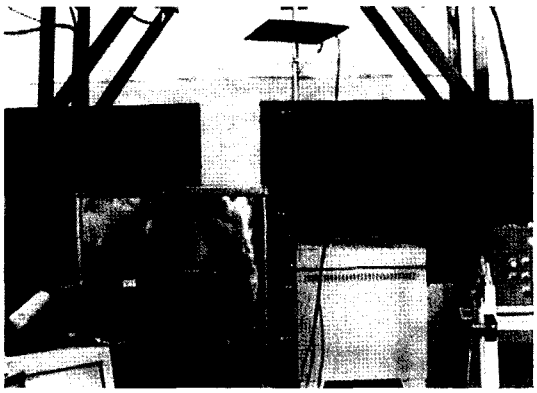

Fig. 3. Picture of DELTA Apparatus

Figure 4 demonstrates the smoothed temperature history in the test section of diameter 120 mm. Initially temperature of the test section decreases through film boiling heat transfer. Thus, the slope of temperature decrease is lax in the film boiling regime. In the transient and nucleate boiling regimes, the temperature drops at a much faster rate on account of enhanced heat transfer.

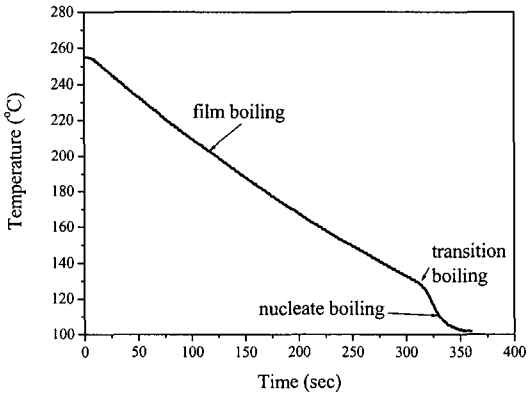

Fig. 4. Temperature History for Test Section of Diameter 120 mm

Figure 5 shows the temperature history for the test section of diameter 294 mm. The temperature regime of film boiling on the larger test section is smaller than that on the smaller. In addition, the Leidenfrost point is higher than that for 120 mm. This may be attributed to the greater conduction heat transfer effect for the larger one. The transition time from the film boiling to nucleate boiling is longer than that for 120 mm.

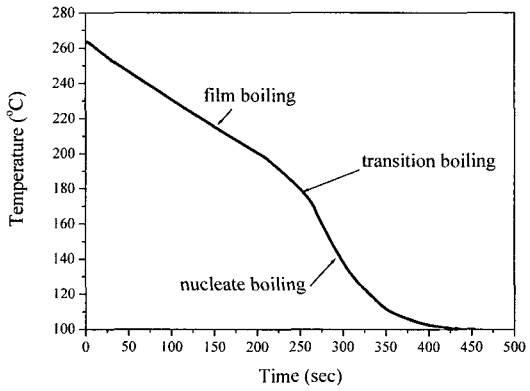

Fig. 5. Temperature History for Test Section of Diameter 294 mm

Figure 6 illustrates the film boiling heat transfer coefficients with the wall superheat for diameter 120 mm, and results from the numerical analysis. The heat transfer coefficients from our experiments lie within the bounding values for cases 1 and 2. The film boiling regime for diameter 120 mm is laminar, but the heat transfer coefficients are closer to those for case 2.

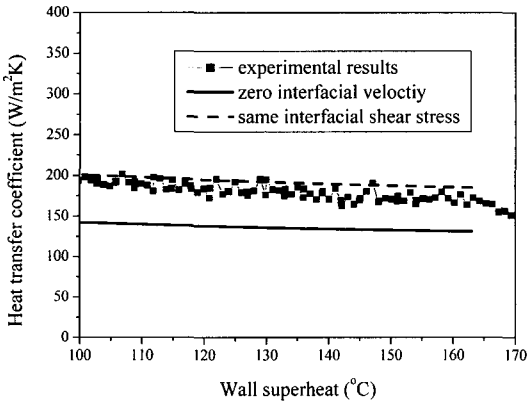

Fig. 6. Film Boiling Heat Transfer Coefficient for Test Section of Diameter 120 mm

Figure 7 depicts the film boiling heat transfer coefficients varying with the wall superheat measured from the diameter 294 mm and predicted by the numerical analysis. The heat transfer coefficients obtained from the tests are greater than those from the numerical analysis for case 2. Thus, the film boiling regime in the DELTA experiment is not simply laminar, but rather involves more complexities like the Helmholtz instability.

Hsu and Westwater [16] estimated the condition for the onset of transition to turbulent flow in film boiling as

$$\mathrm{Re}_{\delta} = \frac{\rho_v u_g \delta}{\mu_v} \tag{19}$$

With increasing angle starting from the bottom, the vapor film continues to thicken, and the vapor flow becomes more turbulent. The interfacial waves accordingly increase in wavelength, eventually becoming unstable. When this occurs the interfacial waves may roll up and break releasing vapor bubbles into the adjacent liquid.

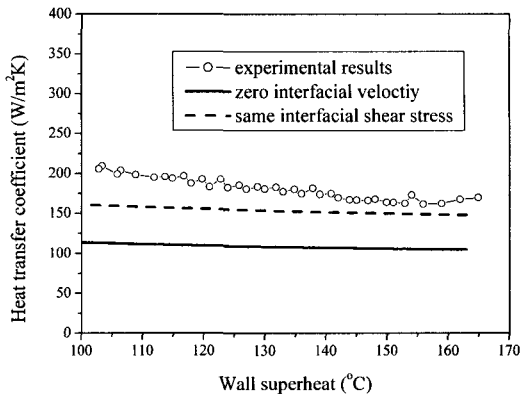

Fig. 7. Film Boiling Heat Transfer Coefficient for Test Section of Diameter 294 mm

Figure 8 presents the vapor film Re for the conditions in the DELTA tests. For the test section with diameter 120 mm, the vapor film Re is always less than 100. Thus, the experimental data lie within the bounding values for cases 1 and 2. The transition angle when the vapor film Re reaches 100 lies between 60° and 70° for the test section with diameter 294 mm. Moreover, the larger the wall superheat, the smaller the transition angle. The laminar film boiling regime covers most part of the downward-facing hemisphere with lower wall superheat in the current test. It may thus be supposed that the test results should be close to predictions by the laminar film boiling analysis. It turns out, on the other hand, that the measured data are greater than the numerical results despite the large transition angle expected for the lower wall superheat in this test. According to Bui and Dhir [8], and Kolev [10], the interfacial wavy motion due to the Helmholtz instability is believed to be the key factor in explaining underprediction of the experimental results by the laminar film boiling analysis. The limiting vapor

film thickness imposed by the Helmholtz instability will tend to increase the film boiling heat transfer due to local breakup of the film.

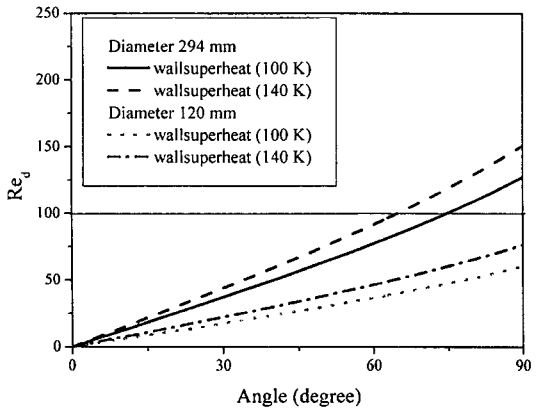

Fig. 8. Vapor Film Reynolds Number for Test Sections

Figure 9 compares the experimental results for the two test sections. Little difference is observed between the two experimental results. It is surmised that similar film boiling heat transfer coefficients result from similar vapor film thickness in the two experiments. The Helmholtz instability limits the vapor velocity and film thickness.

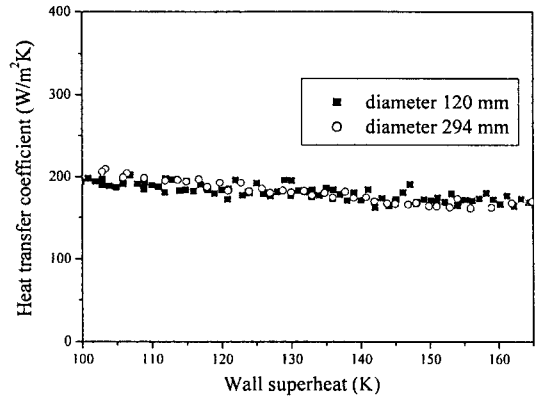

Fig. 9. Comparison of Two Experimental Results

For a wall superheat of 120 K, the heat transfer coefficients obtained from the two diameters are plotted in Figure 10. The experimental data reveal little dependence of the heat transfer coefficient on the diameter. In contrast, the laminar film boiling heat transfer analysis predicts a monotonous reduction in the heat transfer with diameter. For the diameter of 120 mm, the heat transfer coefficient lies within the bounding values for cases 1 and 2 based on the laminar film boiling heat transfer.

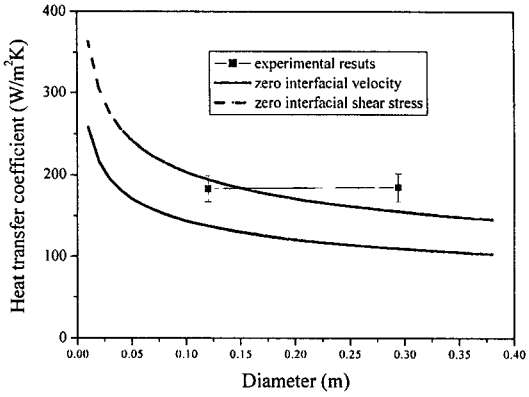

Fig. 10. Comparison of Predicted and Observed Dependence of Heat Transfer Coefficient on Diameter of a Downward-facing Hemisphere

Figure 11 compares El-Genk and Glebov' s experimental results [17] and the laminar film boiling analysis corresponding to their experimental condition. Spanning the whole range of wall superheat, their experimental data lie within the bounding values of cases 1 and 2. The graph indicates that the film boiling regime was laminar in their experiments.

Figure 12 presents the film boiling heat transfer coefficients derived from the two experiments. The diameter of the test section in our experiments is the same as the curvature diameter of the test section in El-Genk and Glebov [17]. However, their test section was not of a full downward-facing hemisphere, but rather a bottom piece whose edge angle was 9.88°. The two test sections are identically made of copper. The film

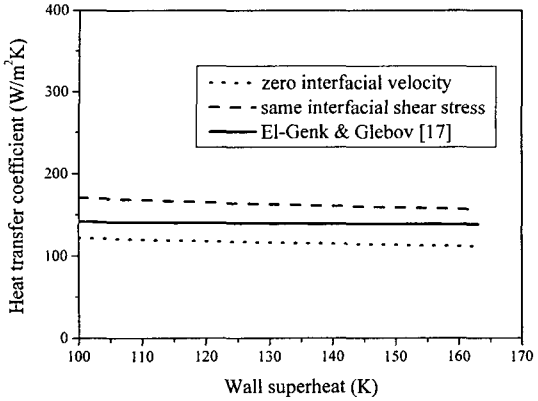

Fig. 11. Comparison of Laminar Film Boiling Heat Transfer and El-Genk and Glebov's [17] Experiments

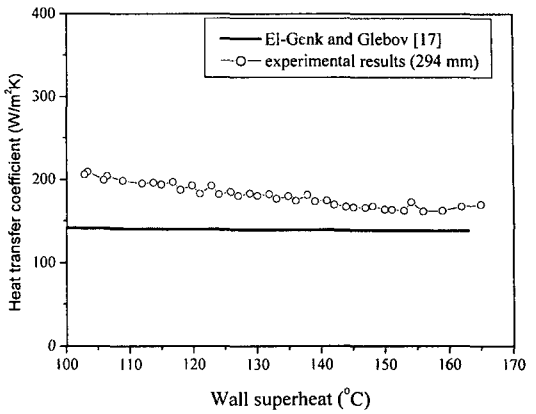

Fig. 12. Comparison of Experimental Data for Test Section of Diameter 294 mm

boiling heat transfer coefficients from our experiments are larger than those from El-Genk and Glebov's experiments [17]. If the film boiling regime were strictly laminar in our experiments, the heat transfer coefficients should have been smaller than those from their experiment. This is because their test section covered only the limited lower portion of the hemisphere, whereas our test section represented the full hemisphere so that the thickening vapor film on the upper portion of the test section must have contributed to deteriorating heat transfer from our test section. It is thence speculated that the film boiling regime for diameter of 294 mm is not simply laminar. Most presumably the interfacial wavy motion plays a pivotal role in augmenting heat transfer from the full hemisphere. In addition, the large edge angle increases the vapor removal on the edge. Hence, the large edge angle is seen to increase the film boiling heat transfer coefficients.

Figure 13 presents the heat flux in relation with the wall superheat. The minimum heat flux is about 20 kW/m^2 for diameter of 294 mm. The value is lower than that reported by El-Genk and Gao [18]. Their experiments for aluminum and 303E stainless steel showed that the minimum heat flux for 303E stainless steel is larger than that for aluminum. Their experiments for aluminum and 303E stainless steel showed that the minimum heat flux for 303E stainless steel is larger than that for aluminum. The Leidenfrost point for 294 mm is higher than that for 120 mm. According to visual observation, destabilization of film boiling propagated radially outward for 120 mm. On the other hand, destabilization spread radially inward for 294 mm. This is due to the difference in the minimum film thickness location between the two test sections. For 120 mm, the location is 0°. However, the interfacial wavy motion due to the Helmholtz instability thins out the vapor film in the upper region. This in turn results in the different Leidenfrost point temperatures and starting points for the film boiling collapse. In addition, the maximum heat flux in our experiment is about 100 kW/m^2 which is lower than the values presented by Cheung et al. [19] and El-Genk and Gao [18]. This is because the thermal conduction heat transfer is ignored in this study. Bi exceeds 0.1 at the maximum heat flux. When the thermal conduction heat transfer is taken into account, the maximum heat flux calculated from our experiment will tend to approach the general critical heat flux.

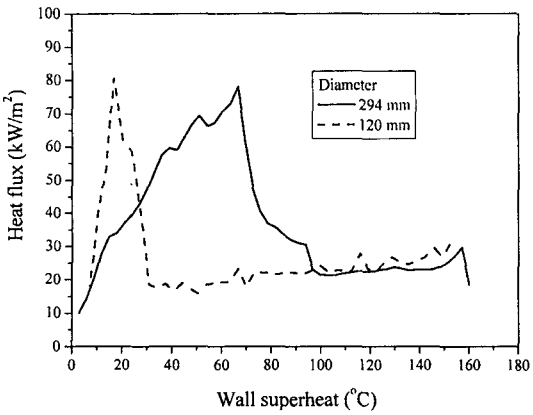

Fig. 13. Boiling Curve with Varying Diameters

5. Conclusions

Film boiling heat transfer coefficients on the downward-facing hemisphere were obtained from the measured temperatures. Major results may be summarized as follows.

(1) The film boiling regime for the test section of diameter 120 mm was laminar, and the heat transfer coefficients were closer to those for the same interfacial shear stress boundary condition.

(2) On the other hand, the film boiling heat transfer coefficients for the test section of diameter 294 mm were greater than those given by the numerical solution for the laminar film boiling due mostly to the Helmholtz instability.

(3) Interfacial wavy motion is considered to be the governing mechanism determining the film boiling heat transfer coefficient in this experiment for diameter 294 mm. Additionally, large vertical edge angle in the full hemisphere increased the film boiling heat transfer coefficients as compared to those for the partial lower segment of the hemisphere.

(4) There was little difference between the film boiling heat transfer coefficients from the two test sections of diameter equal to 120 mm and 294 mm.

(5) For the test section of diameter 120 mm, the Leidenfrost point temperature is lower than that for the test section of diameter 294 mm. Destabilization of film boiling propagated radially inward for 294 mm. On the other hand, destabilization propagated radially outward for 120 mm.

Acknowledgement

This work was performed as part of the Nuclear Safety Analysis National Research Laboratory funded by the Korean Ministry of Science and Technology.

Nomenclature

Bi	Biot number $Bi = h_{film}D/k$
c_p	specific heat of test section
$c_{p,v}$	specific heat of vapor
D	diameter of test section
G	ratio of volume to outer area of test section
g	gravitational acceleration
h_{film}	film boiling heat transfer coefficient
h_{lv}	latent heat of water
h^*_{lv}	effective latent heat of water
h_{rad}	radiation heat transfer coefficient
Ja	Jacob number $Ja = h^*_{lv}/(c_{p,v}\Delta T_{sat})$
k	thermal conductivity of copper
k_v	thermal conductivity of vapor
N_u	Nusselt number $Nu = h_{film}D/K_v$
R	radius of test section
r	radial component in spherical coordinate
R_a	Rayleigh number $Ra = gD^3(\rho_l - \rho_v)/(\mu_v a_v)$
Re_δ	vapor film Reynolds number
T	temperature
T_w	wall temperature

U_{hfilm} uncertainty of film boiling heat transfer coefficient
U_T uncertainty of average temperature in test section
u azimuthal velocity
u_δ interfacial velocity
W_i interfacial mass flow rate
W_l interfacial mass flow rate of liquid
W_v interfacial mass flow rate of vapor

Greek Letters

a_v thermal diffusivity of vapor
ΔT temperature differential during time step
Δt time step size
ΔT_{sat} wall superheat
δ vapor film thickness
θ angular component in spherical coordinate
μ_v viscosity of vapor
ρ density of test section
ρ_l density of liquid
ρ_v density of vapor
τ_i interfacial shear stress
τ_l interfacial shear stress of liquid
τ_v interfacial shear stress of vapor

References

1. L. A. Bromely, "Heat Transfer in Stable Film Boiling," *Chemical Engineering Progress*, 46, 221, (1950).
2. J. C. Koh, "Analysis of Film Boiling on Vertical Surfaces," *Journal of Heat Transfer*, 84, 103, (1962).
3. E. M. Sparrow, R. D. Cess, "The Effect of Subcooled Liquid on Laminar Film Boiling," *Journal of Heat Transfer*, 84, 103 (1962).
4. K. Nishikawa, T. Ito, "Two-Phase Boundary Layer of Free Convection Film Boiling," *International Journal of Heat and Mass Transfer*, 19, 1173 (1966).
5. T. H. Frederking, J. A. Clark, "Natural Convection Film Boiling on a Sphere," *Advanced Cryogenic Engineering*, 8, 501, (1963).
6. A. Sakurai, M. Shiotsu, K. Hata, "A General Correlation for Pool Film Boiling Heat Transfer from a Horizontal Cylinder to Subcooled Liquid: Part 1- A Theoretical Pool Film Boiling Heat Transfer Model Including Radiation Contribution and Its Analytical Solution," *Journal of Heat Transfer*, 112, 430, (1990).
7. S. K. Tou, C. P. Tso, "Improvement on the Modeling of Film Boiling on Spheres," *International Communication of Heat and Mass Transfer*, 24, 6, 879, (1997).
8. T. D. Bui, V. K. Dhir, "Film Boiling Heat Transfer on Vertical Plates and Spheres," *Journal of Heat Transfer*, 107, 764, (1985).
9. V. K. Dhir, G. P. Purohit, "Subcooled Film Boiling Heat Transfer from Spheres," *Nuclear Engineering and Design*, 47, 49, (1978).
10. N. I. Kolev, "Film Boiling on Vertical Plates and Spheres," *Experimental Thermal and Fluid Science*, 18, 97, (1998).
11. J. H. Kim, "Film Boiling Stability and Heat Transfer on Spheres," Ph. D. Thesis, *University of Manchester, England*, (1994).
12. F. P. Incropera, D. P. Dewitt, *Introduction to Heat Transfer*, 3rd ed., Ch. 5, John Wiley and Sons, Inc., New York, NY, USA, (1996).
13. W. Peyayopanakul, J. W. Westwater, "Evaluation of the Unsteady-state Quenching Method for Determining Boiling Curves," *International Journal of Heat and Mass Transfer*, 21, 1437, (1978).
14. V. K. Dhir, "Boiling Heat Transfer," *Annual Review of Fluid Mechanics*, 30, 365, (1998).
15. J. W. Westwater, J. J. Hwalek, M. E. Irving, "Suggested Standard Boiling Curves by Quenching," *Ind. Eng. Chem. Fundam.*, 25, 685, (1986).
16. Y. Y. Hsu, J. W. Westwater, "Approximate

Theory for Film Boiling on Vertical Surfaces," *Chem. Engr. Prog. Symp. Ser.*, 56, 30, 15, (1960).

17. M. S. El-Genk, A. G. Glebov, "Film Boiling from a Downward-Facing Curved Surface in Saturated and Subcooled Water," *International Journal of Heat and Mass Transfer*, 39, 2, 275, (1995).
18. M. S. El-Genk, S. Gao, "Experiments on Pool Boiling of Water from Downward-Facing Hemisphere," *Nuclear Technology*, 125, 52, (1999).
19. F. B. Cheung, K. H. Haddad, Y. C. Liu, "Critical Heat Flux Phenomenon on a Downward Facing Curved Surface," *NUREG/CR-6507 PSU/ME-7321*, (1997).